

Self-injected semiconductor distributed feedback lasers for frequency chirp stabilization

Khalil Kechaou,^{1,*} Frédéric Grillot,^{1,2} Jean-Guy Provost,³ Bruno Thedrez,¹ and Didier Erasme¹

¹Institut Mines-Telecom, Telecom ParisTech, CNRS LTCI, 46 rue Barrault, 75634 Paris Cedex, France

²Université Européenne de Bretagne, INSA, CNRS- Laboratoire FOTON, 20 avenue des buttes de Coesmes, 35708 Rennes, Cedex 7, France

³III-V Lab, a joint lab of 'Alcatel-Lucent Bell Labs France', 'Thales Research and Technology' and 'CEA Leti', Route de Nozay, 91460 Marcoussis, France

*khalil.kechaou@telecom-paristech.fr

Abstract: It is well known that semiconductor distributed feedback lasers (DFB) are key devices for optical communications. However direct modulation applications are limited by the frequency chirp induced by current modulation. We demonstrate that a proper external control laser operation leads to chirp-to-power ratio (CPR) stabilization over a wide range of modulation frequencies as compared to the free-running case. Under experimentally selected optical feedback conditions, the CPR decreases significantly in the adiabatic regime from about 650 MHz/mW in the solitary case down to 65 MHz/mW. Experimental results are also confirmed by numerical investigations based on the transfer matrix method. Simulations point out the possible optimization of the CPR in the adiabatic regime by considering a judicious cavity design in conjunction with a proper external control. These results demonstrate important routes for improving the transmission performance in optical telecommunication systems.

©2012 Optical Society of America

OCIS codes: (140.3490) Distributed-Feedback lasers; (140.5960) Semiconductor lasers.

References and Links

1. K. Petermann, *Laser Diode Modulation and Noise* (Kluwer Academic Publisher, 1991).
2. K. Kechaou, T. Anfray, K. Merghem, C. Aupetit-Berthelemot, G. Aubin, C. Kazmierski, C. Jany, P. Chanclou, and D. Erasme, "Improved NRZ transmission distance at 20 Gbit/s using dual electroabsorption modulated laser," *Electron. Lett.* **48**(6), 335–336 (2012).
3. D. Mahgerefteh, Y. Matsui, X. Zheng, and K. McCallion, "Chirp managed laser and applications," *IEEE J. Sel. Top. Quantum Electron.* **16**(5), 1126–1139 (2010).
4. J. Binder and U. Kohn, "10 Gbits/s-dispersion optimized transmission at 1,55 μm wavelength on standard single mode fiber," *IEEE Photon. Technol. Lett.* **6**(4), 558–560 (1994).
5. N. A. Naderi, F. Grillot, V. Kovanis, and L. F. Lester, "Simultaneous low linewidth enhancement factor and high bandwidth quantum-dash injection-locked laser," *International Photon. Conf. Arlington, USA* (2011).
6. F. Grillot, B. Thedrez, J. Py, O. Gauthier-Lafaye, V. Voiriot, and J. L. Lafrayette, "2.5-Gb/s transmission characteristics of 1.3- μm DFB lasers with external optical feedback," *IEEE Photon. Technol. Lett.* **14**(1), 101–103 (2002).
7. D. M. Kane and K. A. Shore, *Unlocking Dynamical Diversity* (Wiley, 23–54, 2005).
8. N. Schunk and K. Petermann, "Numerical analysis of the feedback regimes for a single-mode semiconductor laser with external feedback," *IEEE J. Quantum Electron.* **24**(7), 1242–1247 (1988).
9. R. W. Tkach and A. R. Chraplyvy, "Regimes of feedback effects in 1.5- μm distributed feedback lasers," *J. Lightwave Technol.* **4**(11), 1655–1661 (1986).
10. D. Lenstra, B. H. Verbeek, and A. J. Den Boef, "Coherence collapse in single-mode semiconductor lasers due to optical feedback," *IEEE J. Quantum Electron.* **21**(6), 674–679 (1985).
11. C. Henry and R. F. Kazarinov, "Instabilities of semiconductor lasers due to optical feedback from distant reflectors," *IEEE J. Quantum Electron.* **22**(2), 294–301 (1986).
12. J. Mork, B. Tromborg, and J. Mark, "Chaos in semiconductor lasers with optical feedback: theory and experiment," *IEEE J. Quantum Electron.* **28**(1), 93–108 (1992).

13. J. Mork, B. Tromborg, and P. L. Christiansen, "Bistability and low-frequency fluctuations in semiconductor lasers with optical feedback: a theoretical analysis," *IEEE J. Quantum Electron.* **24**(2), 123–133 (1988).
14. G. Duan, P. Gallion, and G. Debarge, "Analysis of frequency chirping of semiconductor lasers in the presence of optical feedback," *Opt. Lett.* **12**(10), 800–802 (1987).
15. F. Grillot, B. Thedrez, F. Mallecot, C. Chaumont, S. Hubert, M. F. Martineau, A. Pinquier, and L. Roux, "Analysis, fabrication and characterization of 1.5 μm selection-free tapered stripe DFB lasers," *IEEE Photon. Technol. Lett.* **14**(8), 1040–1042 (2002).
16. J. G. Provost and F. Grillot, "Measuring the chirp and the linewidth enhancement factor of optoelectronic devices with a mach-zehnder interferometer," *IEEE Photon. J.* **3**(3), 476–488 (2011).
17. R. Schimpe, J. E. Bowers, and T. L. Koch, "Characterization of frequency response of 1.5- μm InGaAsP DFB laser diode and InGaAs PIN photodiode by heterodyne measurement technique," *Electron. Lett.* **22**(9), 453–454 (1986).
18. L. Olofsson and T. G. Brown, "Frequency dependence of the chirp factor in 1.55 μm distributed feedback semiconductor lasers," *IEEE Photon. Technol. Lett.* **4**(7), 688–691 (1992).
19. L. A. Coldren and S. W. Corzine, *Diode Lasers and Photonic Integrated Circuits* (Wiley, 1995).
20. G. P. Agrawal, "Effect of gain nonlinearities on the dynamic response of single-mode semiconductor lasers," *IEEE Photon. Technol. Lett.* **1**(12), 419–421 (1989).
21. G. P. Agrawal, *Semiconductor Lasers* (Van Nostrand Reinhold, 1993)
22. P. Vankwikelberge, F. Buytaert, A. Franchois, R. Baets, P. Kuindersma, and C. W. Fredriksz, "Analysis of the carrier-induced FM response of DFB lasers: Theoretical and Experimental case studies," *IEEE J. Quantum Electron.* **25**(11), 2239–2254 (1989).
23. B. Thedrez, J. M. Rainsant, N. Aberkane, B. Andre, H. Bissessur, J. G. Provost, and B. Fernier, "Power and facet phase dependence of chirp for index and gain-coupled DFB lasers," paper TuE41, Semiconductor Laser Conference, 175–176 (1998).
24. F. Grillot, B. Thedrez, and G.-H. Duan, "Feedback sensitivity and coherence collapse threshold of semiconductor DFB lasers with complex structures," *IEEE J. Quantum Electron.* **40**(3), 231–240 (2004).
25. F. Grillot, B. Thedrez, O. Gauthier-Lafaye, M. F. Martineau, V. Voiriot, J. L. Lafrayette, J. L. Gentner, and L. Silvestre, "Coherence collapse threshold of 1.3 μm semiconductor DFB lasers," *IEEE Photon. Technol. Lett.* **15**(1), 9–11 (2003).
26. B. Tromborg, H. Olesen, X. Pan, and S. Saito, "Transmission line description of optical feedback and injection-locking for Fabry-Perot and DFB lasers," *IEEE J. Quantum Electron.* **23**(11), 1875–1889 (1987).
27. A. Lestra and P. Brosnon, "Design rules for a low-chirp integrated DFB laser with electroabsorption modulator," *IEEE Photon. Technol. Lett.* **8**(8), 998–1000 (1996).
28. K. Bjork and O. Nilsson, "A new exact and efficient numerical matrix theory of complicated laser structures: properties of asymmetric phase-shifted DFB lasers," *J. Lightwave Technol.* **5**(1), 140–146 (1987).
29. I. Orfanos, T. Sphicopoulos, A. Tsigopoulos, and C. Caroubalos, "A tractable above-threshold model for the design of DFB and phase-shifted DFB lasers," *IEEE J. Quantum Electron.* **27**(4), 946–956 (1991).
30. L. V. Asryan and R. A. Suris, "Longitudinal spatial hole burning in a quantum-dot laser," *IEEE J. Quantum Electron.* **36**(10), 1151–1160 (2000).

1. Introduction

Today, lower cost and lower consumption optical sources are required for the deployment of access and metropolitan networks and for supporting new services like HDTV (High-Definition television), VOD (Video-On-Demand) as well as Cloud-computing. In response to this demand, directly Modulated Distributed Feedback Lasers (DM-DFB) used as 10 Gb/s transmitters offer compactness, high output power, convenient optical bandwidth and cost efficiency. It is, however, well known that DFB lasers suffer from significant frequency shift (chirp) under current modulation conditions. For high-speed applications, this frequency chirp has been shown to broaden the modulated spectrum, a serious limitation in optical fiber communications [1]. In this context, a lot of research activities are focusing on how to overcome the dispersion limit for 1.55- μm signal. Several methods and devices have been developed with the aim of extending the transmission reach. These include Electro-absorption Modulated Lasers (EMLs) and more recently Dual modulation [2] and Chirp Managed Laser (CML) [3] schemes. These two latter techniques rely on tuning the adiabatic chirp according to the Binder and Kohn's condition [4].

It has been shown recently that the laser's adiabatic chirp can be reduced by zeroing the linewidth enhancement factor (α_H -factor) through injection-locking under strong optical injection [5]. Therefore, a new approach to enhance the transmission distance may consist in monitoring the DFB laser's adiabatic chirp through external control techniques. The scope of this paper is to theoretically and experimentally demonstrate a stabilization of the frequency

chirp over a wide range of modulation frequencies based on a suitably controlled external optical feedback. The investigation is carried out using a conventional quantum well (QW) based DFB laser through an analysis of the chirp to power ratio (CPR).

Self-injection (or external optical feedback) [6] is known to strongly alter the performance of a semiconductor laser. Small reflections in the percent range which originate from launching laser light in an optical fiber or any other optical can dramatically affect the laser stability [7]. Although external optical feedback can be considered as a source of instability, it also can improve the laser performance. For instance, it can be used to reduce the laser's linewidth and can be applied to encryption based on chaos, frequency tuning or velocity measurements [7,8]. Five distinct regimes characterized by spectral observation have been reported in the case of 1.55- μm distributed feedback (DFB) semiconductor lasers [9]. One possible consequence of the external feedback is coherence collapse [10]. When the external feedback exceeds a certain level, the laser becomes unstable and the coherence of the laser output is dramatically reduced. Before the coherence collapse regime, the behavior of the laser linewidth with increasing feedback strength starts with a reduction followed by a rebroadening. In practice external feedback when coupled into the laser cavity through the output facet, causes a modification of the photon density. This perturbation leads to a fluctuation in the carrier density affecting the optical gain. Since the fluctuations of optical refractive index are directly related to the carrier density [11], the external feedback also introduces phase fluctuations. The interaction of the intensity and phase fluctuations makes the dynamics of the laser system under self-injection very complex leading to system instabilities and even chaos. The coherence collapse regime has been described as some co-existing chaotic attractors and as an important source of noise [12] [13]. For lasers used as an optical transmitter, the coherence collapse causes intolerable bit-error-rate degradations [6]. Although the impact of the different feedback regimes in semiconductor laser's nonlinear dynamic has led to a wide range of theoretical and experimental papers, none of them have investigated really the relationship between the CPR and the laser linewidth enhancement factor. To this end, let us cite a theoretical work [14] in which the control of the CPR with self-injection was explicitly pointed out. However, the results published in this study were only theoretical and limited to the short external cavity regime.

This paper shows that in the case of a long external cavity, the CPR can remain constant over a wide range of modulation frequencies, which is of first importance for future optical communication systems. Under optimum feedback conditions the CPR does not exceed an average value of ~ 100 MHz/mW from 10 kHz to 10 GHz, which corresponds to a reduction by a factor of 6.3 when compared to the solitary case. In order to provide insight on the observed chirp stabilization, self-consistent calculations based on the transfer matrix method provide a good qualitative agreement with the experiments. Numerical simulations also reveal that the sensitivity to external optical feedback of an antireflection/high reflection coated (AR/HR) DFB laser depends strongly on the Bragg grating coefficient, which controls the amplitude of Spatial Hole Burning (SHB). In addition, different laser chirp behaviors are observed according to the optical feedback conditions. Furthermore the Bragg grating coefficient as well as the facets reflectivities is shown to influence the adiabatic CPR magnitude.

2. Experimental results

The QW DFB laser under study is a buried ridge stripe (BRS) structure with a HR coating on the rear facet and an AR coating on the front facet, which provide a high external efficiency. The device is 350 μm long with an active layer consisting of six InGaAsP QWs separated by 10 nm wide barriers. The QWs are 8 nm wide and have a 1.1% compressive strain. The grating is defined in a passive quaternary layer localized over the active region and was measured to be about 30 cm^{-1} ($\kappa L \sim 0.8$). A conventional holographic process is used to fabricate a single pitch grating over the full wafer [15]. The threshold current value is $I_{th} = 8$

mA with an external efficiency $\eta = 0.26$ W/A at 25°C. The objective of the experiments is to determine all the characteristics of the frequency modulation (FM) contribution induced by current modulation and under optical feedback conditions.

The CPR as well as the linewidth enhancement factor has been measured using the experimental set-up shown in Fig. 1. The implementation of the optical feedback loop is based on a 4-port optical coupler. Emitted light is launched into port 1 using a lensed fiber. The optical feedback is created with a high-reflectivity coated fiber in port 3 and controlled via a variable optical attenuator (VOA). Its magnitude is determined by measuring the optical power coming out port 2. Then port 4 is connected directly to a Mach-Zehnder (MZ) interferometer constituted of two fibered couplers for chirp measurements. The CPR extraction is based on the frequency and amplitude modulation (FM and AM) characteristics induced by the laser current modulation. The interferometer free-spectral range is equal to the inverse of the time-delay between the two arms. In order to finely control the optical path difference, a cylindrical piezoelectric transducer is used. The transducer located onto one MZ arm is directly controlled by an external locking circuit. The interferometer operating point can be tuned so as to reach all the values included in one period of its sinusoidal frequency response. In the linear region of the characteristic, the photocurrent variations coming out from the photodetector are directly proportional to the frequency variations of the optical signal to be analyzed for a constant optical power. The complex CPR related to the FM/AM ratio can then be extracted both in phase and in amplitude [16].

A polarization controller (PC) matches the feedback beam's polarization to that of the emitted wave in order to maximize the effects. The magnitude of the feedback is defined as the ratio $\Gamma = P_1/P_0$ of the power returned to the facet and launched into the cavity P_1 over P_0 the emitted one. The feedback is studied for a long external cavity [7] given by $\omega_r\tau \gg 1$ where τ and ω_r are the external round trip time (in the order of several hundred nanoseconds) and the laser relaxation frequency (a few GHz). Measurements are made for a bias current equal to $2.4 \times I_{th}$, which corresponds to an emitting power of $P_0 \approx 3$ mW. The coupling loss coefficient between the laser output and the optical fiber was kept constant at ~ 3 dB during the entire experiment. Since the external cavity is long, all feedback regimes could not be observed. The optical spectrum was monitored using a 10 pm high-resolution optical spectrum analyzer.

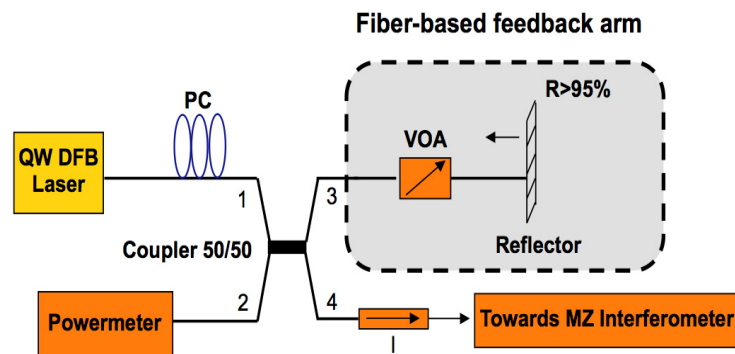


Fig. 1. Schematic of the optical feedback loop

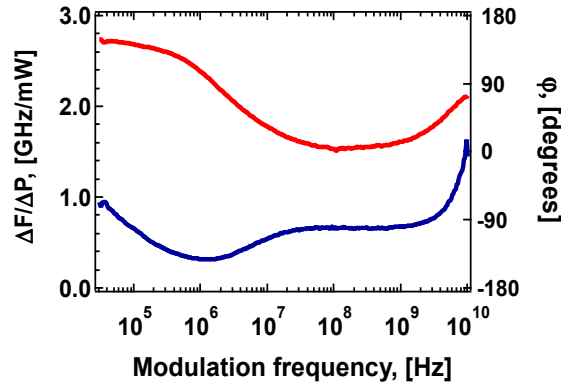


Fig. 2. Amplitude (blue) and phase (red) of the CPR as a function of the modulation frequency for the solitary QW DFB laser.

Figure 2 shows the amplitude (blue) and the phase (red) of the CPR as a function of the frequency modulation for the solitary QW DFB laser emitting at 1550 nm. At low frequencies ($\omega/2\pi < 10$ MHz), thermal effects are predominant. For instance, at 30 kHz, the amplitude and the phase of the CPR are ~ 1.0 GHz/mW and $\sim 140^\circ$ respectively. Within the range $10 \text{ MHz} < \omega/2\pi < 1 \text{ GHz}$, amplitude (AM) and FM modulations are in-phase (adiabatic regime) and the amplitude of the CPR reaches 650 MHz/mW at $\omega/2\pi = 500$ MHz. In that case, thermal effects are no longer significant compared to the refractive index effects induced by the modulation of the carrier density. When $\omega/2\pi > 1 \text{ GHz}$, relaxation oscillations between the carrier and photon numbers lead to a transient chirp with larger CPR values of about 1.5 GHz/mW at 10 GHz and a phase difference approaching 90° .

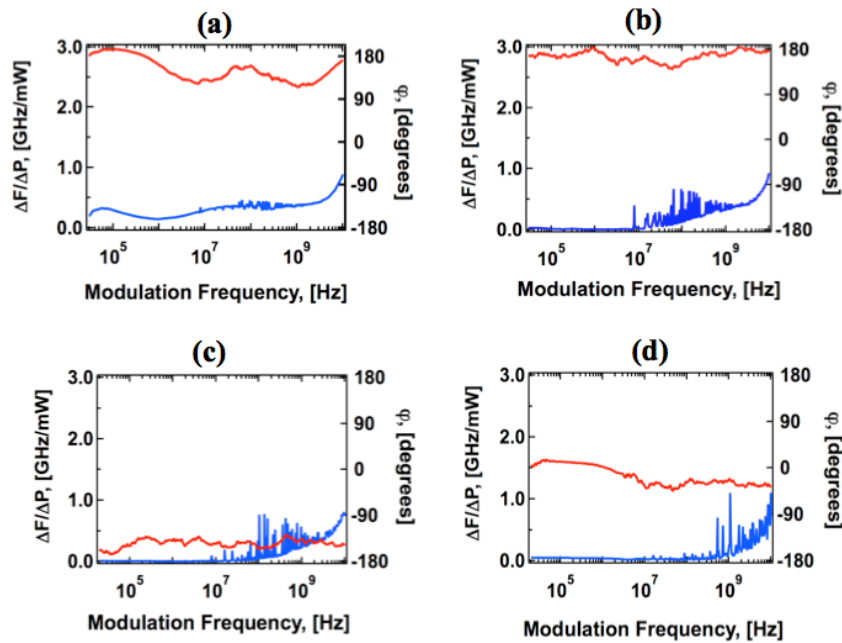


Fig. 3. Amplitude (blue) and phase (red) of the CPR as a function of the modulation frequency for various optical feedback Γ (a) $\Gamma = 1.4 \times 10^{-6}$, (b) $\Gamma = 1.5 \times 10^{-5}$, (c) $\Gamma = 1.6 \times 10^{-4}$, and (d) $\Gamma = 5.5 \times 10^{-3}$.

Figure 3 displays both the amplitude and the phase of the CPR for various feedback levels (a) $\Gamma = 1.4 \times 10^{-6}$, (b) $\Gamma = 1.5 \times 10^{-5}$, (c) $\Gamma = 1.6 \times 10^{-4}$, and (d) $\Gamma = 5.5 \times 10^{-3}$. The results demonstrate that the use of a controlled optical feedback can modify both the thermal and adiabatic chirps. Firstly, the averaged CPR measured in the thermal regime is significantly decreased from about 565 MHz/mW in the solitary case down to 33 MHz/mW at the highest feedback level. Secondly, the CPR measured in the adiabatic regime at $\omega/2\pi = 500$ MHz ranges from about 650 MHz/mW in the solitary case down to 65 MHz/mW at the highest feedback level. Under the selected optical feedback condition ($\Gamma = 5.5 \times 10^{-3}$) the CPR does not exceed ~ 100 MHz/mW on average from 10 kHz to 10 GHz, which corresponds to a reduction by a factor of 6.3 when compared to the solitary case. Figure 4 illustrates the stabilization of the measured adiabatic CPR at $\omega/2\pi = 500$ MHz as a function of the optical feedback strength.

Figure 3 illustrates also the transient chirp modifications resulting from the self-injected field. For instance, for $\omega/2\pi = 10$ GHz, the transient chirp is improved by a factor of 2 compared to the free-running case. However, the amplitude of the optical feedback has to be controlled carefully in order to avoid the parasitic peaks seen in Fig. 3 arising when the modulation frequency gets close to the relaxation frequency. These are related to external cavity modes. Let us note that the laser remained single longitudinal mode throughout the measurements. Severe unstable regimes such as the exaltation of the relaxation oscillations leading to the chaotic state regime was not observed except for the last data point in Fig. 4 ($\Gamma = 1.5 \times 10^{-2}$).

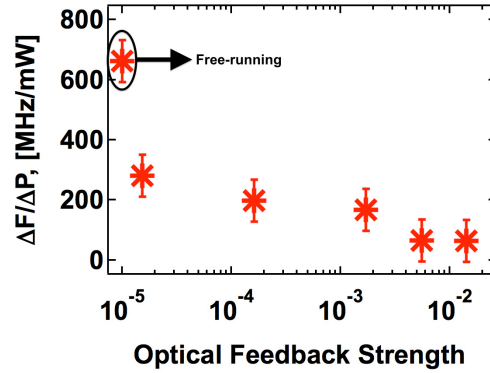


Fig. 4. CPR in the adiabatic regime measured at 500 MHz as a function of the optical feedback strength for the QW DFB laser.

In order to explain the observed CPR amplitude variations we have also investigated the linewidth enhancement factor variations induced by optical feedback. Figure 5 shows the measured $2\beta/m$ (with $\beta \equiv \Delta F/f_m$ and $m \equiv \Delta P/P_0$, with $f_m = \omega/2\pi$) ratio as a function of the modulation frequency. The linewidth enhancement factor is extracted from this ratio through the relationship [17],

$$\frac{2\beta}{m} = \alpha_H \sqrt{1 + \left(\frac{\omega_c}{\omega}\right)^2} \quad (1)$$

In (1), the roll-off frequency $\omega_c/2\pi$ is defined as the corner frequency [18],

$$f_c = \frac{1}{2\pi} v_g \frac{\partial g}{\partial P} P \quad (2)$$

with v_g the group velocity, P the output power and $\partial g/\partial P$ is a nonzero parameter related to finite intraband relaxation times as well as carrier heating. The parameter $\partial g/\partial P$ can be expanded as a function of the gain compression factor ϵ following the relationship [19]:

$$\frac{\partial g}{\partial P} = \frac{\epsilon g}{1 + \epsilon P} \quad (3)$$

For typical devices, the corner frequency is in the hundreds of MHz to few GHz range depending on the output power level. Thus, for high modulation frequencies such as $\omega \gg \omega_c$, a condition which is easily reached in our experiments (the maximum modulation frequency is around 20 GHz), $2\beta/m$ directly equals to the laser's linewidth enhancement factor. For low modulation frequencies, the ratio $2\beta/m$ becomes inversely proportional to the modulation frequency.

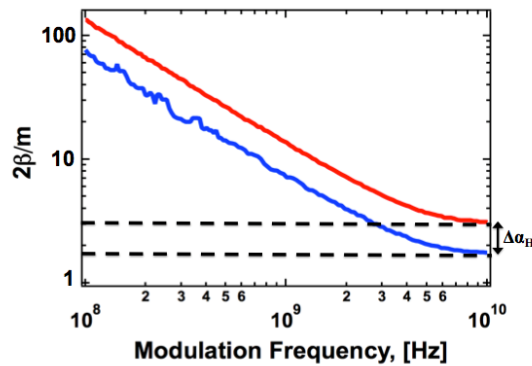


Fig. 5. Measured $2\beta/m$ ratio as a function of the modulation frequency for the solitary case (red plot) and for an optical feedback of about $\Gamma = 1.5 \times 10^{-5}$ optical feedback (blue plot).

In Fig. 5, the measured $2\beta/m$ ratio is plotted starting from 50 MHz (beyond the thermal effects) for the solitary case (red plot) and for a feedback level of about $\Gamma = 1.5 \times 10^{-5}$ (blue plot). As predicted by (1), $2\beta/m$ tends asymptotically to the linewidth enhancement factor value, which is estimated to be about 3.2 in the absence of external perturbation. The modification of the linewidth enhancement factor under self-injection can be explained by the change of the threshold carrier density induced by optical feedback. The measured linewidth enhancement factor decreases down to about 1.8, which can indeed explain the chirp reduction magnitude. Independently of optical feedback, the roll-off frequency was graphically determined to be about 4.5 GHz from Fig. 5. The variations of $2\beta/m$ with optical output power can also be used to evaluate the gain compression factor ϵ . Based on reference [20], the compression factor is estimated for the solitary laser under study to be about 0.15 mW^{-1} , which is in good agreement with previous published values on similar laser structures [21].

Figure 3 shows that the external control induces a modification not only in the CPR's modulus but also in the CPR's phase due to optical feedback, FM versus AM modulations can be approximately out of phase (Fig. 3(b)) or in-phase (Fig. 3(d)). Consequently, in these situations, the sign of the adiabatic CPR can be negative or positive. Such a change indicates some routes for engineering the laser's chirp and carrying out dispersion management at the source level. Adiabatic chirp of different signs have already been reported in DFB lasers [22,23]. The physical origin of the sign variation is strongly related to the spatial hole burning through the phase effects occurring at the laser facets that are modified in our case by the external field [24,25]. In the following sections, the influence of the self-injection on both the adiabatic CPR sign and amplitude is investigated and compared to experimental results.

3. Model

Let us now consider the situation for which the external reflection is produced on the AR coated side of an AR/HR DFB laser. A self-injected semiconductor laser can be described using the Lang and Kobayashi rate equation [1] as follows:

$$\frac{dE}{dt} = \left[j\omega + \frac{1}{2}(1 + j\alpha_H)(G - 1/\tau_p) \right] E(t) + KE(t - \tau) \quad (4)$$

with $E(t) = \sqrt{S(t)} e^{j(\varphi(t) + \omega_0 t)}$ the complex electrical field which depends on the photon density $S(t)$, the phase $\varphi(t)$ and the free-running laser frequency $\omega_0/2\pi$. In Eq. (4), $\omega_0/2\pi$ is the laser frequency in the presence of external optical feedback, G the modal gain, α_H the linewidth enhancement factor, τ_p the photon lifetime and τ the external roundtrip time. The strength of the delayed field is denoted by the parameter K , which can be expressed as [1]:

$$K = \frac{2C_{AR}\gamma}{\tau_i} \quad (5)$$

with τ_i being the internal roundtrip time within the laser's cavity, γ the amplitude reflectivity of the delayed field ($\Gamma = \gamma^2$) originating from a distant reflecting point and being assumed to be such that $\gamma \ll 1$ with C_{AR} being the coupling strength coefficient of the AR-facet [24]. Under optical feedback the effective reflectivity $r_{AR,eq}$ can also be defined as follows [25]:

$$r_{AR,eq} = \tilde{r}_{AR} e^{-j\phi_{AR}} + (1 - |\tilde{r}_{AR}|^2) \sqrt{\gamma} e^{-j\omega\tau} = \tilde{r}_{AR,eq} e^{j\phi_{AR,eq}} \quad (6)$$

where ϕ_{AR} is the facet phase term describing the position of the facet with respect to the Bragg reflector. The feedback does not affect the description of the HR-facet whose reflectivity can be written:

$$r_{HR,eq} = \tilde{r}_{HR} e^{-j\phi_{HR}} \quad (7)$$

where ϕ_{HR} is the phase term describing the position of the facet with respect to the Bragg reflector. The dynamic evolution of the carrier density is governed by the usual relation:

$$\frac{dN}{dt} = \frac{I(t)}{e} - \frac{N(t)}{\tau_e} - GP(t) \quad (8)$$

where $N(t)$, τ_e , and $I(t)$ respectively are the carrier density within the active zone, the carrier density lifetime and the pump current respectively. In what follows Eq. (6) will be used to evaluate the feedback sensitivity of DFB lasers through the determination of the CPR in the adiabatic regime for several effective front facet reflectivities. Although the numerical simulations do not explicitly incorporate the delayed field occurring in Eq. (4), the approach based on the complex effective reflectivity has already been used to analyze both the static and dynamic DFB lasers properties operating under external control [24,26,27].

The numerical calculations presented below are based on the transfer matrix method (TMM) [28]. The aim is to calculate the QW based DFB laser performance at threshold and to predict its static behavior above threshold with and without feedback. The method is applicable to any laser design. The DFB laser structure is divided into N sections consisting of many grating periods in which all physical parameters, like the injection current, the material gain, the photon density, the carrier density and the refractive index are assumed to be homogeneous. The laser is modeled by assuming the Bragg grating has a rectangular shape. The transfer matrix for one corrugation period is defined by:

$$\overline{M}_{Period} = \begin{bmatrix} \frac{n_1 + n_2}{2n_1} & \frac{n_1 - n_2}{2n_1} \\ \frac{n_1 - n_2}{2n_1} & \frac{n_1 + n_2}{2n_1} \end{bmatrix} \times \begin{bmatrix} e^{k_2 l} & 0 \\ 0 & e^{-k_2 l} \end{bmatrix} \times \begin{bmatrix} \frac{n_1 + n_2}{2n_2} & \frac{n_2 - n_1}{2n_2} \\ \frac{n_2 - n_1}{2n_2} & \frac{n_1 + n_2}{2n_2} \end{bmatrix} \times \begin{bmatrix} e^{k_1 l} & 0 \\ 0 & e^{-k_1 l} \end{bmatrix} \quad (9)$$

where n_1 and n_2 are the refractive indices, and k_1 and k_2 are the complex propagation constants in the two refractive index regions. The real part of the propagation constant is determined by the net gain. The imaginary part depends on refractive index, which affects the frequency shift of the laser. The laser is divided into m sections where the carrier density is kept uniform. The carrier density may however vary from section to section. Section i contains m_i corrugation periods. The complete transfer matrix describing the DFB laser with coated facets is written as:

$$\overline{M} = \overline{r}_{HR} \times \overline{\varphi}_{HR} \times \prod_{i=1}^{i=N} (\overline{M}_{Period})^{m_i} \times \overline{\varphi}_{AR,eq} \times \overline{r}_{AR,eq} \quad (10)$$

where m_i is the number of period in the i th section, \overline{r}_{HR} and $\overline{r}_{AR,eq}$ are the reflectivity matrices at the left and right side, $\overline{\varphi}_{HR}$ and $\overline{\varphi}_{AR,eq}$ are the partial propagation matrices corresponding to incomplete corrugation periods at the left and right facets. To take into account the external feedback, the reflectivity and partial propagation matrices are defined according to Eqs. (6) and (7) by:

$$\overline{r}_{HR,eq} = \frac{1}{\sqrt{1 - \tilde{r}_{HR}^2}} \begin{bmatrix} 1 & -\tilde{r}_{HR} \\ -\tilde{r}_{HR} & 1 \end{bmatrix} \quad (11)$$

$$\overline{r}_{AR,eq} = \frac{1}{\sqrt{1 - \tilde{r}_{AR,eq}^2}} \begin{bmatrix} 1 & \tilde{r}_{AR,eq} \\ \tilde{r}_{AR,eq} & 1 \end{bmatrix} \quad (12)$$

$$\overline{\varphi}_{HR} = \begin{bmatrix} e^{-j\varphi_{HR}} & 0 \\ 0 & e^{-j\varphi_{HR}} \end{bmatrix} \quad (13)$$

$$\overline{\varphi}_{AR,eq} = \begin{bmatrix} e^{j\varphi_{AR,eq}} & 0 \\ 0 & e^{j\varphi_{AR,eq}} \end{bmatrix} \quad (14)$$

The nonlinear field gain can be well approximated by a logarithmic formula including the gain compression effect in the vicinity of the emission frequency:

$$g(N, P) = \frac{g_0 \cdot \ln \left(\frac{ed_{qw} B_{rad} N^2}{J_0} \right)}{1 + \varepsilon P} \quad (15)$$

In this approximation, g_0 , e , d_{qw} , B_{rad} , J_0 , ε , N and P are respectively the empirical gain coefficient, the electron charge, the thickness of one quantum well, the radiative recombination coefficient, the transparency current density, the gain compression coefficient,

the carrier density and the photon density, respectively. For the TMM, the oscillation condition at threshold is computed by using:

$$\overline{M}_{11}(\alpha_{DFB}, \lambda) = 0 \quad (16)$$

A prediction-corrector method has been used to calculate the lasing mode represented by $(\alpha_{th}, \lambda_{th})$. The initial guesses (α_i, λ_i) of solutions correspond to Fabry-Perot modes. After calculating the value of \overline{M}_{11} for (α_i, λ_i) , $(\alpha_i + d\alpha, \lambda_i)$ and $(\alpha_i, \lambda_i + d\lambda)$, we compute the relative variations allowing the correction of the values of α and λ . This procedure is iteratively repeated until a relative variation less than 10^{-9} is reached.

Above threshold, the carrier distribution along the cavity shifts from uniform to non-uniform leading to intra-cavity SHB. The resulting spatial index variation locally affects the grating, which becomes slightly non-uniform. This leads to a deviation of the cavity modes consistent with the new distribution of the refractive index. The above threshold resolution method is described in reference [29]. For uniformly injected current, an iterative procedure is adopted. It consists on the resolution of the oscillation condition (16) using the new photon and carrier density distribution calculated from the previous solutions of the steady-state carrier rate Eq. (8) at lower injected current. The resulting index variation is given by:

$$n(z) = n^{th} + \Gamma_c \frac{dn}{dN} (N(z) - N_{th}) \quad (17)$$

where n^{th} is the refractive index at threshold, Γ_c is the confinement factor, N_{th} is the carrier density at threshold and dn/dN is the slope of the refractive index with respect to the carrier density. The newly obtained solution (α, λ) leads to another distribution of photons and carriers. Therefore, we solve again (16). All steps are repeated until reaching an unchanged (α, λ) . All parameters used in simulation are given in Table 1 below.

Table 1. Simulation parameters of AR/HR-DFB laser

Parameters	Symbol	Value	Unit
Lasing wavelength	λ	1550	nm
Active layer's length	L	350	μm
Quantum Well's number	N_{QW}	6	
Quantum Well's thickness	d_{qw}	0.008	μm
Active layer's width	w	1.3	μm
Effective index	n_{eff}	3.2	
Group index	n_g	3.8	
Bragg grating period	A	$2.42 \cdot 10^{-7}$	m
Confinement factor	Γ_c	0.139	
Gain compression coefficient	ϵ	$3 \cdot 10^{-17}$	cm^3
Internal loss	α_{int}	19	cm^{-1}
Refractive index's slope	dn/dN	$-2.2 \cdot 10^{-20}$	cm^3
Empirical gain coefficient	g_0	800	cm^{-1}
Transparency current density	J_0	50	A/cm^2
Non-radiative recombinaison coefficient	A_{nrad}	0	s^{-1}
Radiative recombinaison coefficient	B_{rad}	$8 \cdot 10^{-11}$	cm^3/s
Auger recombinaison coefficient	C_{aug}	$2 \cdot 10^{-29}$	cm^6/s
Spontaneous emission factor	β_{sp}	10^{-4}	
Linewidth enhancement factor	α_H	3	

4. Numerical results

Using the TMM, a systematic study of the CPR in the adiabatic regime of the DFB laser is first performed. The high reflection facet phase ϕ_{HR} is chosen in order to fit the experimental results. The antireflection coefficient measured on a calibration sample is estimated to be in

the 0.1% range. Thus, the front facet is assumed to be perfectly antireflection coated ($\tilde{r}_{AR} = 0$) so that Eq. (6) can be reduced to:

$$r_{AR,eq} = \sqrt{\gamma} e^{-j\omega\tau} = \tilde{r}_{AR,eq} e^{j\phi_{AR,eq}} \quad (18)$$

In this case, the variation of the effective reflectivity is related directly to the feedback amplitude. Simulations have been conducted assuming $0\% < R_{AR,eq} = |r_{AR,eq}|^2 = \gamma < 4\%$. The simulated CPR in the adiabatic regime of the DFB laser under study is plotted in Fig. 6 as a function of the output power for $\phi_{HR} \approx 0.9\pi$ and various values of effective reflectivity $R_{AR,eq}$ hence various feedback power. The output power is varied through the bias current.

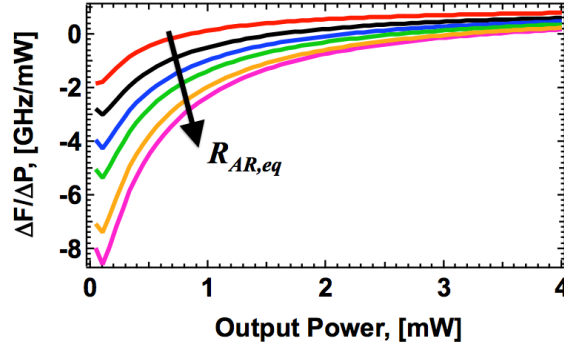


Fig. 6. Calculated CPR in the adiabatic regime as a function of the output power for various feedback conditions ($0\% < R_{AR,eq} = |r_{AR,eq}|^2 = \gamma < 4\%$) and for $\kappa L = 0.8$, $\phi_{HR} \approx 0.9\pi$

At low output power, the CPR is definitely power dependent because of the HR-facet phase effect [23]. Indeed, the optical field's longitudinal distribution changes from uniform at threshold to non-uniform as the power increases, leading to a longitudinal variation of the carrier density. As a consequence, the refractive index and hence the periodic profile of the Bragg reflector is altered, leading ultimately to a wavelength shift. In the present case ($\phi_{HR} < \pi$), the lasing wavelength shifts towards the red. Because of the large grating coefficient, the introduction of the feedback does not affect the typical CPR power dependence but it can, however, affect its magnitude, at a fixed output power. The distribution of the internal optical power is sensitive to the effective reflection coefficient leading to a significant dependence of the CPR on the feedback strength. Hence, for a 1mW output power, the absolute value of the CPR increases from 0 to 2 GHz/mW when $R_{AR,eq}$ varies from 0% to 4%. At higher output powers, the CPR converges towards a positive value around 730 MHz/mA independent of the facet phase and of the feedback condition. This value is given by [1]:

$$k = \frac{\eta_i \alpha_H \Gamma_c \mathcal{E}}{e 4\pi V} \quad (19)$$

where η_i is the internal quantum efficiency and $V = N_{QW} d_{QW} L w$ the cavity volume. Equation (19) describes the wavelength shift induced by the gain compression effect. At high output power, the index profile gets stabilized, and the SHB induced wavelength shift gradually disappears. The remaining wavelength shift is then only due to gain compression, which happens not to be feedback dependent.

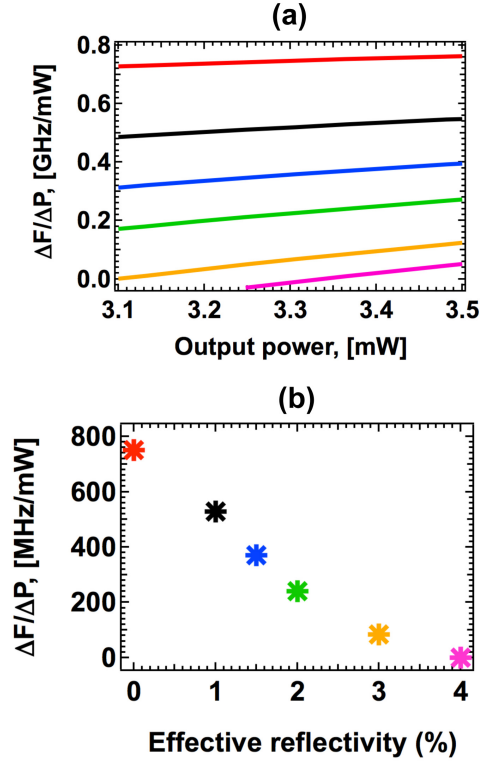


Fig. 7. (a) Zoom from Fig. 6 showing the calculated CPR in the adiabatic regime as a function of the output power for various feedback conditions ($\kappa L = 0.8$); (b) Calculated CPR in the adiabatic regime as a function of the effective front facet reflectivity ($\kappa L = 0.8$, $P_0 = 3.36$ mW).

Figure 7(a) shows a zoom from Fig. 6 for output powers between 3.1 and 3.5 mW displaying clearly that the optical feedback has a strong impact on the adiabatic CPR. Figure 7(b) depicts the simulated values of the adiabatic CPR at $P_0 = 3.4$ mW (colored markers) as a function of the effective facet reflectivity which is in that case related to the optical feedback strength through Eq. (18). One can notice that simulated CPR drops from 750 MHz/mW for $R_{AR,eq} = 0\%$ (solitary case) to 65 MHz/mW with $R_{AR,eq} \approx 3\%$. These variations are in good qualitative agreement with the experimental results depicted in Fig. 4. From a quantitative point of view, the optical feedback range explored in the experiments differs from the simulations. Such a discrepancy can be attributed mostly to the fact that the numerical simulations consider feedback in terms of optical power and not in terms of delayed field. Further numerical studies should investigate the impact of the delay on the laser's dynamics through a resolution of Eq. (4) in amplitude and phase.

From Fig. 7(a), one can see that the sign of the adiabatic chirp can change when the effective reflectivity increases (larger feedback). This effect is even more drastic when one reduces the Q -factor of the cavity (lower κL). Figure 8 shows the calculated adiabatic CPR for a grating coupling coefficient of $\kappa L = 0.5$ with $L = 350$ μm . In this case, the front facet reflectivity is 0.1% (green plot), 0.5% (black plot), 1% (red plot) and 2% (blue plot) respectively. Compared to Fig. 6, decreasing (κL) leads to an increase of the laser's sensitivity to the optical feedback.

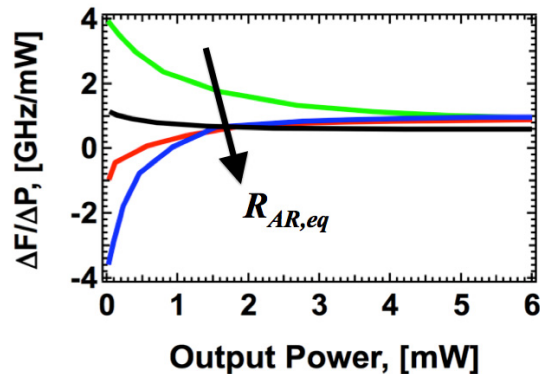


Fig. 8. Calculated CPR in the adiabatic regime as a function of the output power for various feedback conditions for $\kappa L = 0.5$ and $L = 350 \mu\text{m}$. Front facet reflectivity is 0.1% (green), 0.5% (black), 1% (red) and 2% (blue) respectively.

As an example, Fig. 8 displays the CPR for $\kappa L = 0.5$. When the front facet reflectivity is increased, the adiabatic CPR at 1 mW drastically decreases from about 2 GHz/mW down to 45 MHz/mW. One can also observe two types of CPR power dependence, similar to the measurements of reference [23], which include a change of the curvature. Figure 8 points out that if the optical feedback strength gets sufficiently large, the adiabatic CPR can change sign and turn from blue (green curve) to red (blue curve). As a result, controlling optical feedback allows one to minimize or to zero the adiabatic CPR. This situation results from a proper design of the laser cavity design associated to a well-tuned delayed field having the required properties both in amplitude and in phase.

5. Conclusion

The chirp induced by the optical modulation of a QW DFB diode laser is evaluated through the measurement of the CPR. Experimental results have demonstrated that under optimum optical feedback conditions the adiabatic CPR decreases significantly from about 650 MHz/mW in the solitary case down to 65 MHz/mW. This realization is of importance for improving the transmission performance in optical communication systems. Such experimental results are confirmed by numerical investigations based on the transfer matrix method. Simulations have also pointed out the possibility of optimizing the adiabatic CPR by considering a judicious cavity design in addition to a proper external control. Further studies should investigate the effects of the optical feedback on the chirp under large signal analysis as well as in quantum dot nanostructure based semiconductor lasers for which the SHB effects have been demonstrated to be larger [30].

Acknowledgments

The authors are grateful to the MODULE project from the French national initiative ANR-VERSO program and SYSTEMATIC Paris-Region for financial support. Special thanks also to Dr. Mark Crowley from the University of New-Mexico (USA) for his valuable comments on the paper. Dr. Frédéric Grillot's work is supported in part by the European Office of Aerospace Research and Development (EOARD) under grant FA8655-12-1-2093.